*materials*

MDPI

*Article*

# A New BCN Compound with Monoclinic Symmetry: First-Principle Calculations

**Zhenyang Ma [1,2], Chunzhi Tang [1,2,*] and Chunlei Shi [1,2]**

[1] Key Laboratory of Civil Aircraft Airworthiness Technology, Civil Aviation University of China, Tianjin 300300, China; zyma@cauc.edu.cn (Z.M.); clshi01@126.com (C.S.)
[2] College of Safety Science and Engineering, Civil Aviation University of China, Tianjin 300300, China
* Correspondence: cz_tang0302@126.com

**Abstract:** In this study, we predicted and investigated a new light-element compound B-C-N in *Pm* phase, denoted as *Pm*-BCN, using density functional theory. *Pm*-BCN is mechanically, dynamically, and thermodynamically stable. The elastic moduli of *Pm*-BCN are larger than those of other B-C-N and light-element compounds, such as $P2_13$ BN, $B_2C_3$, $P4/m$ BN, *Pnc*2 BN, and dz4 BN. By studying the mechanical anisotropy of elastic moduli, we proved that *Pm*-BCN is a mechanically anisotropic material. In addition, the shear anisotropy factors $A_2$ and $A_{Ba}$ of *Pm*-BCN are smaller than those of the seven B-C-N compounds mentioned in this paper. *Pm*-BCN is a semiconductor material with an indirect and wide band gap, suggesting that *Pm*-BCN can be applied in microelectronic devices.

**Keywords:** carbon allotropes; semiconductor material; electronic properties; anisotropy mechanical properties



**Citation:** Ma, Z.; Tang, C.; Shi, C. A New BCN Compound with Monoclinic Symmetry: First-Principle Calculations. *Materials* **2022**, *15*, 3186. https://doi.org/10.3390/ma15093186

Academic Editors: Jason Shian-Ching Jang, Shou-Yi Chang and Lijun Zhang

Received: 7 March 2022
Accepted: 24 April 2022
Published: 28 April 2022



## 1. Introduction

Designing new light-element atoms based on boron, carbon, and nitrogen, which easily form strong covalent bonds to form compounds, is an important method of finding new multifunctional materials. New theoretically proposed materials include superhard materials [1–16], direct bandgap materials [17,18], hydrogen and lithium storage materials [19,20], and metal materials that can be used for the preparation of battery cathode materials [1,4,21,22].

Three new carbon allotropes with an orthogonal structure, *o*P-$C_{16}$, *o*P-$C_{20}$, and *o*P-$C_{24}$, were proposed based on first-principles calculations [1], all of which showed metallicity. The hardness of *o*P-$C_{16}$, *o*P-$C_{20}$, and *o*P-$C_{24}$ are 47.5, 49.6, and 55.3 GPa, respectively. The ideal shear strengths of *o*P-$C_{16}$, *o*P-$C_{20}$, and *o*P-$C_{24}$ are higher than those of Cu and Fe, and Al. Yu et al. [23] predicted and studied a new $sp^2$ hybrid BN polymorph, *Pnc*2 BN, which showed mechanical and dynamic stability, and found that the elastic properties of *Pnc*2 BN are better than those of dz4 BN. The indirect band gap of *Pnc*2 BN calculated using the Heyd–Scuseria–Ernzerhof (HSE06) functional is 3.543 eV, indicating that *Pnc*2 BN has semiconductor properties. On the basis of density functional theory (DFT) calculations [24,25], *m*-$B_3CN_3$ and *m*-$B_2C_3N_2$, two new superhard BCN compounds, were designed by Xing et al. [5]. The shear modulus *B*, bulk modulus *G*, and Young's modulus *E* of *m*-$B_3CN_3$ and *m*-$B_2C_3N_2$ are 345, 778, and 346, respectively; the *B*, *G*, and *E* for *m*-$B_3CN_3$ and *m*-$B_2C_3N_2$ are little bit larger than those of *o*-$BC_6N$ [2], *t*-$BC_6N$-1 [2], and *t*-$BC_6N$-2 [2]. Both *m*-$B_3CN_3$ and *m*-$B_2C_3N_2$ are superhard materials because both compounds have a hardness in excess of 40 GPa. The structural properties, anisotropy characteristics, elastic characteristics, and electronic properties, as well as the stability, of $P4/m$ BN were investigated by Yu et al. [26]. By adopting DFT, Xing et al. established and studied CN and $BCN_2$ compounds with superhard characteristics and a space group of $C2/m$ [4]. The hardness of CN is 58.63 GPa, and it is a semiconductor material, whereas $BCN_2$ is metallic. A superhard material, *t*-$C_8B_2N_2$, was designed by Zhu et al. [10] and Wang et al. [11]. The bulk modulus

of *t*-$C_8B_2N_2$ was found to be 383.4 [10] and 383.0 GPa [11], and the hardness was 64.7 [10] and 63.2 GPa [11].

In this study, we predicted a BCN polymorph, *Pm* BCN, which is mechanically and dynamically stable. We analyzed the structural, mechanical, and electronic characteristics of *Pm* BCN through first-principles calculations.

## 2. Theoretical Methods

On the basis of DFT calculations [24,25], we proposed and investigated a new light-element compound using the Cambridge Serial Total Energy Package (CASTEP) [27]. We adopted the generalized gradient approximation (GGA) with the Perdew–Burke–Ernzerhof (PBE) [28] and local density approximation (LDA) [29] functionals to describe the exchange and correlation potentials. To ensure that the crystal structure of *Pm*-BCN was optimal, we used Broyden–Fletcher–Goldfarb–Shanno (BFGS) [30] for geometry optimization. The convergence accuracy during optimization was less than 0.001 eV. We described the valence electrons by ultrasoft pseudopotentials [31]. We adopted the Monkhorst–Pack *k*-points for the *k*-points separation of 6 × 16 × 7 and found that the plane wave cut-off energy $E_{\text{cut-off}}$ is 500 eV for *Pm*-BCN. For the phonon spectra of *Pm*-BCN, we used the density functional perturbation theory (DFPT) approach [32], and for the electronic band structures of *Pm*-BCN, we adopted the HSE06 hybrid functional [33]. In addition, we used the Voigt–Reuss–Hill (VRH) approximations [34–36] to calculate the bulk modulus and shear modulus.

## 3. Results and Discussion

The crystal structure of *Pm*-BCN and its structure along the *b*-axis are shown in Figure 1a,b, respectively. Blue, gray, and purple spheres represent the B, N, and C atoms, respectively. In addition to the common rings such as the 4- and 6-membered rings in the crystal structures of *Pm*-BCN, two larger rings, a 10- and a 16-membered ring, are present in the crystal structure, the structures of which are depicted in Figure 1c,d. The 4-membered ring consists of one B, one N, and two C atoms; the 6-membered ring consists of one B, one N, and four C atoms; the 10-membered ring consists of three B, three N, and four C atoms. The 16-membered ring consists of five B, five N, and six C atoms. The conventional *Pm*-BCN cell contains 12 atoms. Because *Pm*-BCN has a monoclinic system, the crystal structure of *Pm*-BCN is not symmetrical, and the position of each atom is different. Boron atoms occupy four positions: B1 1*a* (0.11803, 0.00000, and 0.20845), B3 1*a* (0.22107, 0.00000, and 0.73817), B10 1*b* (0.80293, 0.50000, and 0.62435), and B12 1*b* (0.59805, 0.50000, and 0.04251); nitrogen atoms occupy four positions: N2 1*a* (0.78254, 0.00000, and 0.74717), N7 1*b* (0.18971, 0.50000, and 0.61515), N8 1*b* (0.87536, 0.50000, and 0.36710), and N11 1*b* (0.40657, 0.50000, and 0.04285); and carbon atoms occupy four positions: C4 1*a* (0.88003, 0.00000, and 0.20041), C5 1*a* (0.71892, 0.00000, and 0.01576), C6 1*a* (0.29294, 0.00000, and 0.01183), and C9 1*b* (0.11385, 0.50000, and 0.37443). Table 1 shows the crystal lattice parameters of the B-C-N compounds. The crystal lattice parameters of *Imm*2 BCN and *I*-4*m*2 BCN are close to those previously reported [14]; therefore, the crystal lattice parameters of *Pm*-BCN reported in this manuscript are both convincing and reliable.

The stability of *Pm*-BCN through phonon spectra (Figure 2a), relative enthalpy (Figure 2b), and elastic parameters. In Figure 2a, no curve appears below zero, so *Pm*-BCN is dynamically stable. We calculated the formation energies of B-C-N compounds as: $\Delta H = H_{\text{B}x\text{C}y\text{N}z}/m\text{-}xH_{\text{c-BN}}/n\text{-}yH_{\text{diamond}}/p$. As several B-C-N compounds have an equal number of nitrogen and boron atoms, here, *x* is equal to *z*; *m*, *n*, and *p* are the $B_xC_yN_z$ unit and atom numbers of the conventional cell for B-C-N compounds, c-BN, and diamond. The formation energy of *Pm*-BCN is 0.7182 eV/atom, which is slightly lower than those of *o*-$BC_6N$-1, *t*-$BC_6N$-2 [2], $B_2C_2N_2$-2, $B_2C_2N_2$-3, $B_2C_2N_2$-4, and $B_2C_2N_2$-5 [38]. We found that the *Pm*-BCN is a metastable phase. Notably, B-C-N compounds with positive formation energies are not unusual [2,4,5,7,8,38].

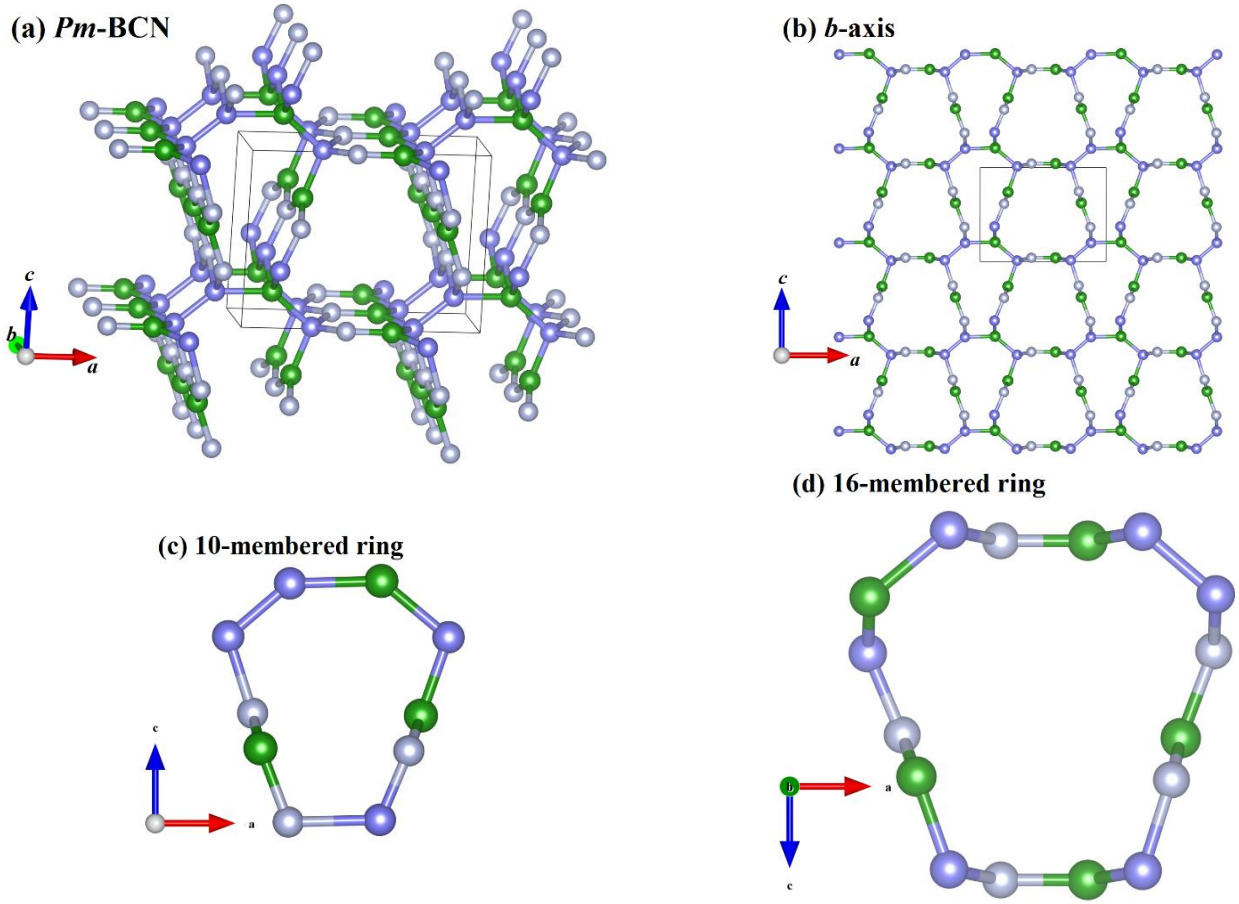


**Figure 1.** Crystal structures of *Pm*-BCN (**a**), Crystal structures of *Pm*-BCN along *b*-axis (**b**), the 10-membered ring structure (**c**), and the 16-membered ring structure (**d**).

**Table 1.** Crystal lattice parameters of *Pm* BCN and other B-C-N compounds.

| | | *a* | *b* | *c* | *β* | *V* | *ρ* |
|---|---|---|---|---|---|---|---|
| *Pm* BCN | GGA | 7.2538 | 2.5387 | 5.4260 | 89.960 | 24.981 | 2.448 |
| | LDA | 7.1697 | 2.5043 | 5.3334 | 89.219 | 23.938 | 2.555 |
| *t*-$C_8B_2N_2$ | GGA [a] | 2.5470 | | 10.9470 | | 17.781 | 3.402 |
| | LDA [b] | 2.5250 | | 10.8540 | | 17.092 | 3.539 |
| *Imm*2 BCN | GGA | 2.5451 | 2.5658 | 10.9077 | | 17.808 | 3.434 |
| | GGA [c] | 2.5453 | 2.5658 | 10.9169 | | 17.822 | |
| | GGA [d] | 2.5480 | 2.5690 | 10.9130 | | 17.859 | |
| | LDA | 2.5129 | 2.5313 | 10.7687 | | 17.125 | 3.571 |
| | LDA [c] | 2.5127 | 2.5309 | 10.7659 | | 17.212 | |
| *I*-4*m*2 BCN | GGA | 2.5648 | | 10.9948 | | 18.081 | 3.382 |
| | GGA [c] | 2.5641 | | 10.9892 | | 18.063 | |
| | GGA [d] | 2.5670 | | 11.0020 | | 18.124 | |
| | LDA | 2.5301 | | 10.8420 | | 17.101 | 3.525 |
| | LDA [c] | 2.5298 | | 10.8396 | | 17.343 | |

[a] [11], [b] [10], [c] [14], [d] [37].

For the monoclinic structure, the Born mechanical stability conditions are [39]: $C_{11} > 0$, $C_{22} > 0$, $C_{33} > 0$, $C_{44} > 0$, $C_{55} > 0$, $C_{66} > 0$, $[C_{11} + C_{22} + C_{33} + 2\,(C_{12} + C_{13} + C_{23})] > 0$, $(C_{33}C_{55} - C_{35}^2) > 0$, $(C_{44}C_{66} - C_{46}^2) > 0$, $(C_{22} + C_{33} - 2C_{23}) > 0$, $[C_{22}\,(C_{33}C_{55} - C_{35}^2) + 2\,C_{23}C_{25}C_{35} - C_{23}^2C_{55} - C_{25}^2C_{33}] > 0$, $\{2[C_{15}C_{25}\,(C_{33}C_{12} - C_{13}\,C_{23}) + C_{15}C_{35}(C_{22}C_{13} - C_{12}C_{23}) + C_{25}C_{35}\,(C_{11}C_{23} - C_{12}C_{13})] - [C_{15}^2(C_{22}C_{33} - C_{23}^2) + C_{25}^2(C_{11}C_{33} - C_{13}^2) + C_{35}^2(C_{11}C_{22} - C_{12}^2)] + C_{55}B\} > 0$, and $B = C_{11}C_{22}C_{33} - C_{11}C_{23}^2 - C_{22}C_{13}^2 - C_{33}C_{12}^2 + 2C_{12}C_{13}C_{23}$. Table 2 lists the

$C_{ij}$ values of *Pm*-BCN and other B-C-N compounds. Table 2 shows that the elastic constants of *Pm*-BCN determined by LDA are slightly higher than those determined by GGA. All the elastic constants of *Pm*-BCN satisfy the above equation for a monoclinic system, proving that *Pm*-BCN is mechanically stable. We calculated the *G* and *B* of B-C-N compounds by using the Voigt–Reuss–Hill approximation [34–36]. The $B_V$, $B_R$, $G_V$, and $G_R$ are given by [38]:

$$B_V = [C_{11} + C_{22} + C_{33} + 2(C_{12} + C_{13} + C_{23})]/9 \quad (1)$$

$$G_V = [C_{11} + C_{22} + C_{33} + 3(C_{44} + C_{55} + C_{66}) - (C_{12} + C_{13} + C_{23})]/15 \quad (2)$$

$$B_R = \Delta[(C_{33}C_{55} - C_{35}^2)(C_{11} + C_{22} - 2C_{12}) + (C_{23}C_{55} - C_{25}C_{35})(2C_{12} - 2C_{11} - C_{23}) + (C_{13}C_{35} - C_{15}C_{33})(C_{15} - 2C_{25}) + (C_{13}C_{55} - C_{15}C_{35})(2C_{12} + 2C_{23} - C_{13} - 2C_{22}) + 2(C_{13}C_{25} - C_{15}C_{23})(C_{25} - C_{15}) + A]^{-1} \quad (3)$$

$$G_R = 15\{4[(C_{33}C_{55} - C_{35}^2)(C_{11} + C_{22} + C_{12}) + (C_{23}C_{55} - C_{25}C_{35})(C_{11} - C_{12} - C_{23}) + (C_{13}C_{35} - C_{15}C_{33})(C_{15} + C_{25}) + (C_{13}C_{55} - C_{15}C_{35})(C_{22} - C_{12} - C_{23} - C_{13}) + (C_{13}C_{25} - C_{15}C_{23})(C_{15} - C_{25}) + A]/\Delta + 3[(C/\Delta) + (C_{44} + C_{66})/(C_{44}C_{66} - C_{46}^2)]\}^{-1} \quad (4)$$

$$A = C_{11}(C_{22}C_{55} - C_{25}^2) - C_{12}(C_{12}C_{55} - C_{15}C_{25}) + C_{15}(C_{12}C_{25} - C_{15}C_{22}) + C_{25}(C_{23}C_{35} + C_{25}C_{33}) \quad (5)$$

$$C = C_{11}C_{22}C_{33} - C_{11}C_{23}^2 - C_{22}C_{13}^2 - C_{33}C_{12}^2 + 2C_{12}C_{13}C_{23} \quad (6)$$

$$\Delta = 2[C_{15}C_{25}(C_{33}C_{12} - C_{13}C_{23}) + C_{15}C_{35}(C_{22}C_{13} - C_{12}C_{23}) + C_{25}C_{35}(C_{11}C_{23} - C_{12}C_{13})] - [C_{15}^2(C_{22}C_{33} - C_{23}^2) + C_{25}^2(C_{11}C_{33} - C_{13}^2) + C_{35}^2(C_{11}C_{22} - C_{12}^2) + (C_{11}C_{22}C_{33} - C_{11}C_{23}^2 - C_{22}C_{13}^2 - C_{33}C_{12}^2 + 2C_{12}C_{13}C_{23})C_{55}] \quad (7)$$

$$B = (B_V + B_R), G = (G_V + G_R) \quad (8)$$

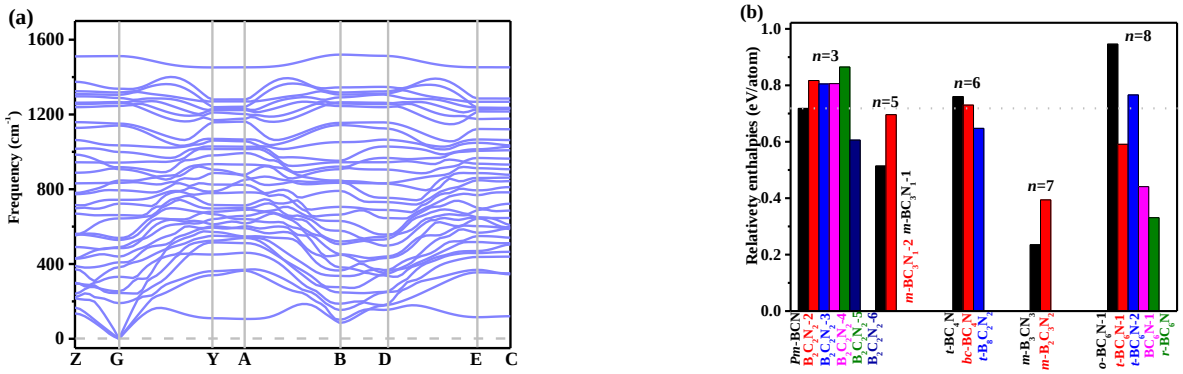


**Figure 2.** Phonon spectra of *Pm*-BCN (**a**) and the relative enthalpies of B-C-N compounds (**b**).

Young's modulus *E* is calculated by $E = 9BG/(3B + G)$, and Table 2 lists the calculated elastic moduli of B-C-N compounds. The elastic moduli of *Pm*-BCN are less than those of other B-C-N compounds, and larger than those of other light element compounds, such as *Pnc*2 BN [23], *P*4/*m* BN [26], $P2_13$ BN [40], $B_2C_3$ [41], dz4 BN [42], etc.

According the ElAM codes [43], we investigated the anisotropic elastic properties of *Pm*-BCN. The *G*, *v*, and *E* are illustrated in Figure 3a–e, respectively. The three-dimensional (3D) graphics of *G*, *v*, and *E* of *Pm*-BCN are not regular spheres, as shown in Figure 3. If a material possesses isotropic properties, its 3D diagram should be a regular sphere, and any shape deviating from a sphere indicates anisotropy [44–50]. So, we found that the *G*, *v*, and *E* of *Pm*-BCN exhibit anisotropic elastic properties. The $G_{max}/G_{min}$ and $E_{max}/E_{min}$ ratios are used to characterize the anisotropic elastic properties of *G* and *E*, which are 207.12/75.11 = 2.76 and 755.31/221.89 = 3.40 for *Pm*-BCN, respectively. As shown by the $G_{max}/G_{min}$ and $E_{max}/E_{min}$ ratios, the anisotropic elastic properties of *Pm*-BCN show that it has a greater shear modulus than $B_2C_3N_2$ and $B_2CN_2$ [5], but a smaller one than $BCN_2$ [4]. $BCN_2$ has the largest Young's modulus among *Pm*-BCN, $B_2C_3N_2$, and $B_2CN_2$; $B_2C_3N_2$ shows the weakest anisotropy in *E*.

**Table 2.** Calculated elastic constants (GPa) and elastic moduli (GPa) of *Pbca* XN, *Imm*2 BCN, and *I*-4*m*2 BCN.

| | | $C_{11}$ | $C_{12}$ | $C_{13}$ | $C_{15}$ | $C_{22}$ | $C_{23}$ | $C_{25}$ | $C_{33}$ | $C_{35}$ | $C_{44}$ | $C_{46}$ | $C_{55}$ | $C_{66}$ | $B$ | $G$ | $E$ |
|---|---|---|---|---|---|---|---|---|---|---|---|---|---|---|---|---|---|
| *Pm* BCN | GGA | 339 | 50 | 184 | 8 | 770 | 48 | 0.4 | 400 | 10 | 194 | 8 | 75 | 189 | 225 | 153 | 374 |
| | LDA | 364 | 61 | 212 | 16 | 829 | 59 | 2 | 405 | 20 | 203 | 12 | 73 | 199 | 245 | 154 | 382 |
| *m*-$B_2C_3N_2$ | GGA [a] | 723 | 97 | 178 | 11 | 936 | 43 | 7 | 871 | 21 | 326 | −2 | 394 | 395 | 351 | 367 | 816 |
| *m*-$B_3CN_3$ | GGA [a] | 684 | 123 | 181 | 21 | 841 | 47 | −7 | 841 | 63 | 304 | 2 | 375 | 387 | 345 | 346 | 778 |
| *t*-$C_8$ $B_2N_2$ | GGA [b] | 987 | 39 | 143 | | | | | 890 | | 368 | | | 389 | 390 | 379 | 858 |
| *Imm*2 BCN | GGA | 963 | 23 | 144 | | 898 | 141 | | 395 | | 395 | | 457 | 343 | 367 | 394 | |
| | GGA [c] | 962 | 22 | 143 | | 894 | 140 | | 819 | | 400 | | 456 | 343 | 365 | 394 | 839 |
| *I*-4*m*2 BCN | GGA | 853 | 45 | 133 | | | | | 753 | | 377 | | | 327 | 342 | 358 | |
| | GGA [c] | 857 | 47 | 135 | | | | | 755 | | 377 | | | 328 | 345 | 358 | 798 |

[a] [5], [b] [10], [c] [14].

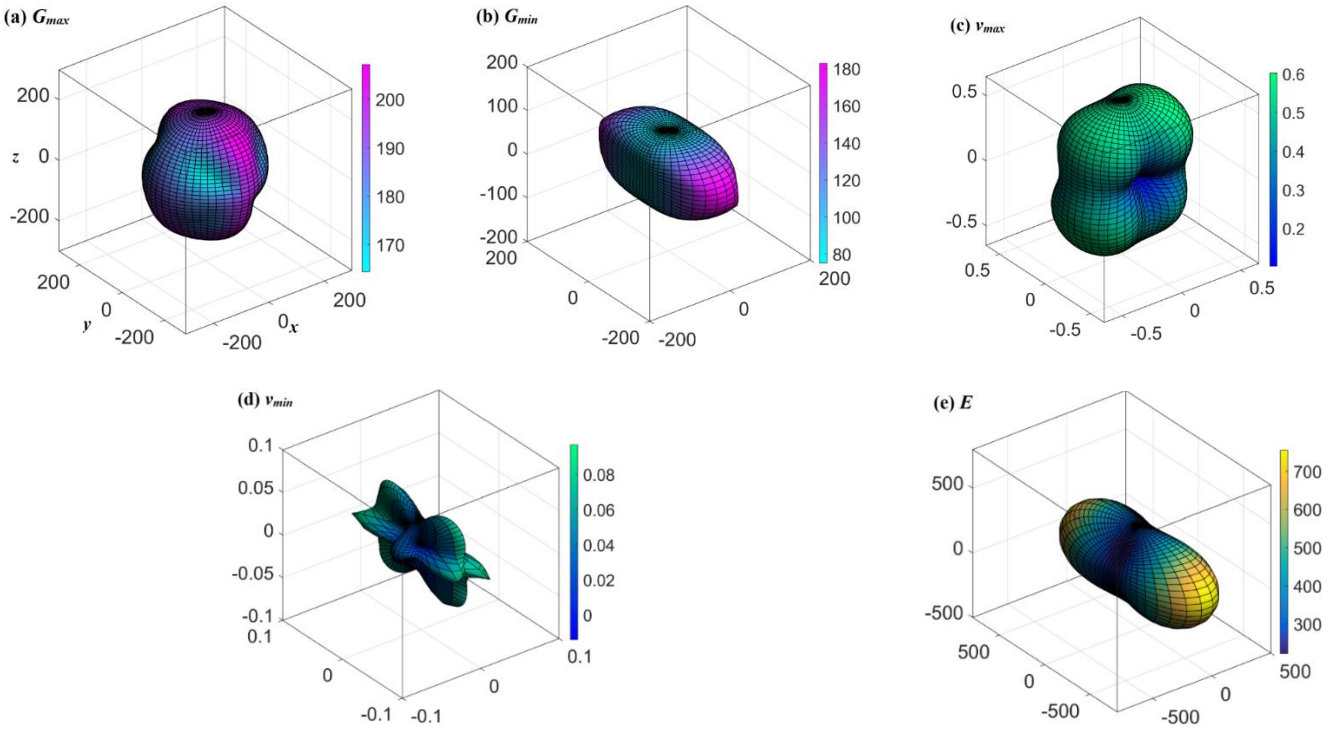


**Figure 3.** Three-dimensional structure of $G_{max}$ (**a**), $G_{min}$ (**b**), Poisson's ratio $v_{max}$ (**c**), $v_{min}$ (**d**), and $E$ (**e**) of *Pm*-BCN.

For mechanical anisotropy in $G$, the shear anisotropy factor is an index of the mechanical anisotropy of atomic bonding in different shear planes. $A_1$, $A_2$, and $A_3$ represent the shear anisotropic factor for the (100) shear plane between [011] and [010] directions, the (010) shear plane between [101] and [001] directions, and the (001) shear plane between [110] and [010] directions, respectively. A1 = 4C44/(C11 + C33 − 2C13), $A_1 = 4C_{55}/(C_{22} + C_{33} - 2C_{23})$, $A_3 = 4C_{66}/(C_{11} + C_{22} - 2C_{11})$ [51,52]. The $A_1$, $A_2$, and $A_3$ of carbon allotropes of seven B-C-N compounds are illustrated in Figure 4a. We found that the $A_1$, $A_2$, and $A_3$ of isotropic materials should be one; however, as shown in Figure 4a, the $A_1$ of *Pm*-BCN is much greater than one, whereas the $A_2$ of *Pm*-BCN is much lower than one, so *Pm*-BCN exhibits a larger anisotropy at the (100) and (010) shear plane. Among these seven B-C-N compounds, the (100), (010), and (001) shear planes of *t*-$C_8B_2N_2$ show minimal differ-

ences, implying that the anisotropies at the three planes of the shear modulus of *t*-$C_8B_2N_2$ are similar. The $B$ along the $a$, $b$, and $c$ axes, $B_a$, $B_b$, and $B_c$, were calculated as [51,53]: $B_a = \Lambda/(1 + \alpha + \beta)$, $B_b = B_a/\alpha$, and $B_c = B_a/\beta$, and $\Lambda = C_{11} + 2C_{12} + C_{22}\alpha^2 + 2C_{13}\beta + C_{33}\beta^2 + 2C_{23}\alpha\beta$, $\alpha = [(C_{11} - C_{12})(C_{33} - C_{13}) - (C_{23} - C_{13})(C_{11} - C_{13})]/[(C_{33} - C_{13})(C_{22} - C_{12}) - (C_{13} - C_{23})(C_{11} - C_{13})]$, and $\beta = [(C_{22} - C_{12})(C_{11} - C_{13}) - (C_{11} - C_{12})(C_{23} - C_{12})]/[(C_{22} - C_{12})(C_{33} - C_{13}) - (C_{12} - C_{23})(C_{13} - C_{23})]$. The anisotropy of the bulk moduli along the $a$ and $c$ directions with respect to the $b$ directions are described by: $A_{Ba} = B_a/B_b$, $A_{Bc} = B_c/B_b$. Figure 4b,c shows the $B_a$, $B_c$, $A_{Ba}$, and $A_{Bc}$ of the seven B-C-N compounds. The $B_a$ and $B_c$ of the seven B-C-N compounds differ. The $B_a$ of $BCN_2$ is the largest, and *Pm*-BCN exhibits the smallest linear bulk modulus $B_a$. Although $BCN_2$ has the largest linear bulk modulus $B_a$, its linear bulk modulus $B_c$ is the smallest. Figure 4c shows that the anisotropy of $B$ along the $a$ direction, $A_{Ba}$, of *t*-$C_8B_2N_2$ and *I*-4*m*2 BCN, and the $A_{Bc}$ of $B_2N_2C_3$ and $B_3N_3C$ are very close to one, indicating that the $B$ of these materials is less anisotropic along the $a$ and $c$ axes. Additionally, *Pm*-BCN exhibits the largest anisotropy in $A_{Ba}$, and $BCN_2$ has the largest anisotropy in $A_{Bc}$.

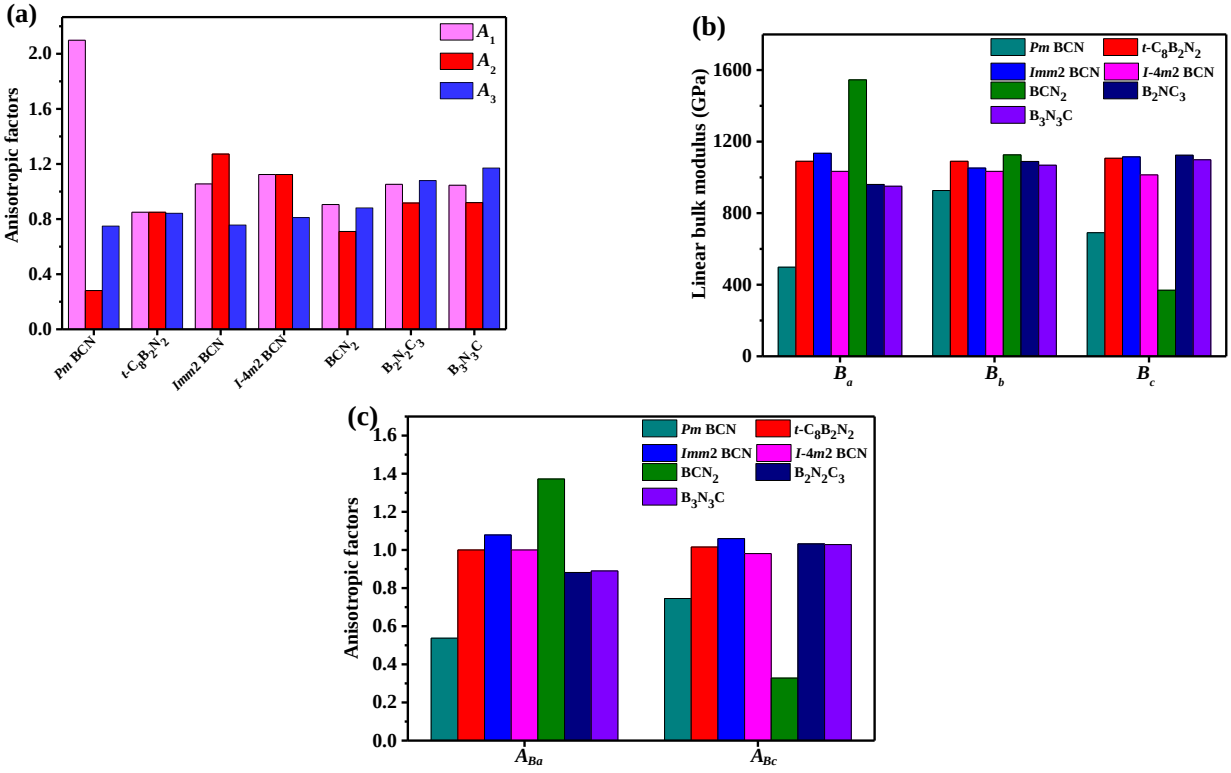


**Figure 4.** Anisotropy factor $A_1$, $A_2$, and $A_3$ (**a**); linear bulk modulus $B_a$, $B_b$, and $B_c$ (**b**); $A_{Ba}$ and $A_{Bc}$ (**c**) for *Pm*-BCN.

The electronic band structure and the PDOS of *Pm*-BCN obtained by the HSE06 function are shown in Figure 5, where the dashed line of zero energy (0 eV) indicates the Fermi level ($E_F$). The valence band maximum (VBM) of *Pm*-BCN is located at Z (0.0, 0.0, 0.5), and its conduction band minimum (CBM) appears at A (0.5, 0.5, 0.0). *Pm*-BCN has an indirect and wide band gap of 2.458 eV, therefore it is clearly a semiconductor. The PDOS can be divided into three parts: the first region ranges from −23 to −18 eV, the second region ranges from approximately −16 eV to the Fermi level, and the third region ranges approximately from 2.5 to 10 eV. The first region is dominated from the *p* orbital, which is primarily from the N-s, C-s, and C-p orbitals. The N-p state and C-s orbitals provide a major contribution to the −16 to −12 eV of the second region. From −12 eV to the Fermi level, the distributions of the B-p, C-p, and N-p orbitals are much greater than that of s orbitals. From 2.5 to 10 eV, the distribution of N-p orbitals is slightly smaller than that

of B-p and C-p orbitals. To further understand the chemical bonds, Figure 6 plots the electron localization function (ELF) of *Pm*-BCN. ELF is an excellent measure of the strength of covalent bonds. Here, B-C and B-N bonding are strongly covalent, whereas the C-N bonding is weakly covalent. The band decomposed charge densities of VBM and CBM of *Pm*-BCN are depicted in Figure 6b,c, respectively. The B atom is the main contributor to the CBM; the C atom contributes a small amount to the CBM but is the main contributor to the VBM; and the N atom makes a small contribution to the VBM.

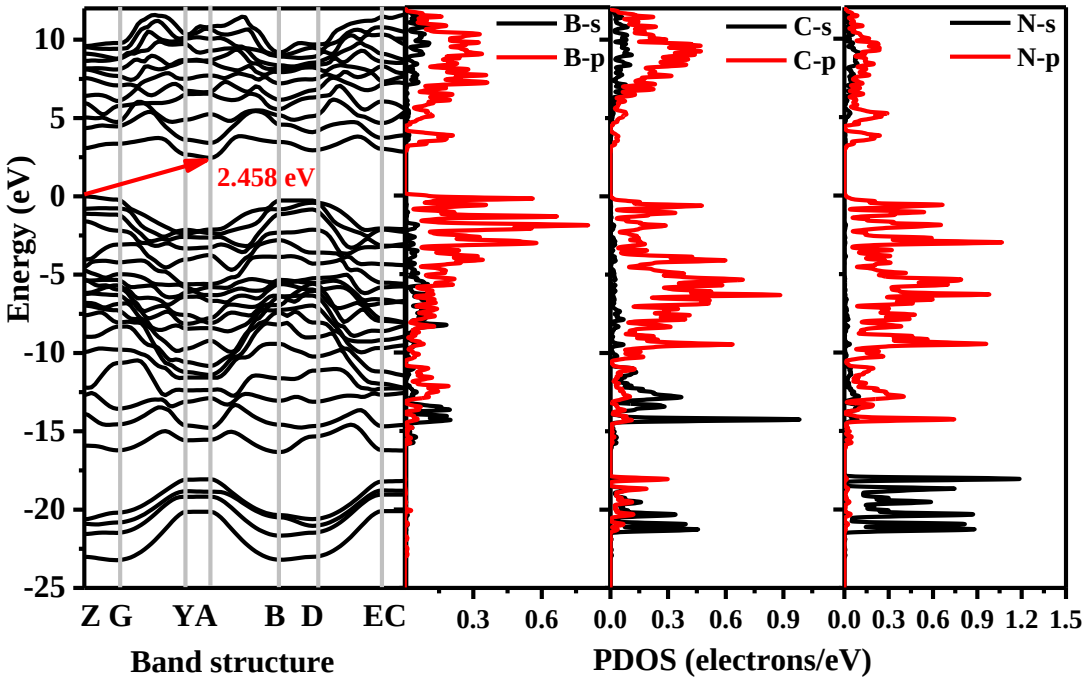


**Figure 5.** Band structure and the partial density of states (PDOS) of *Pm*-BCN.

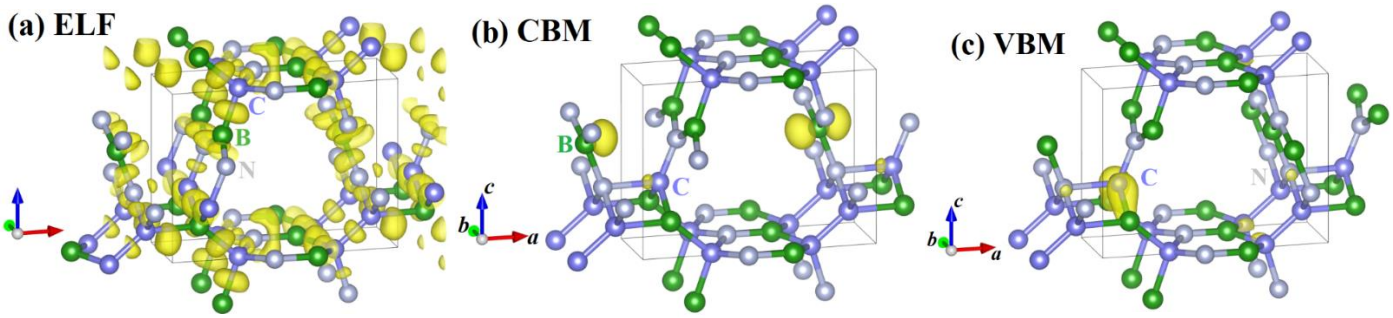


**Figure 6.** Electronic localization functions (**a**) and band decomposed charge densities of VBM and CBM (**b**,**c**) of *Pm*-BCN.

## 4. Conclusions

Based on DFT calculations, in this study, we designed and predicted a new light-element compound, *Pm*-BCN. First, by analyzing the phonon spectrum, we found that the elastic constants and relative enthalpy of *Pm*-BCN are theoretically stable. Second, we found that *Pm*-BCN has an indirect and wide band gap and is a semiconductor material. Third, we showed that the B10 position is the main contributor to the CBM, the C9 position provides a small contribution to the CBM but the main contribution to the VBM, and the N8 position is a minor contributor to the VBM. Finally, we found that the elastic anisotropy in $E$ and the $G$ of *Pm*-BCN are slightly smaller than those of $BCN_2$ according to $E_{max}/E_{min}$ and $G_{max}/G_{min}$, whereas the shear anisotropy factor $A_2$ and the anisotropy of $B$ along the $a$

direction with respect to the *b* direction $A_{Ba}$ of *Pm*-BCN are smaller than those of *t*-$C_8B_2N_2$, *I*-4*m*2 BCN, *Imm*2 BCN, $B_2N_2C_3$, $BNC_2$, and $B_3N_3C$.

**Author Contributions:** Investigation, Z.M., C.T. and C.S.; Writing—original draft, Z.M. and C.T.; Writing—review & editing, C.S. All authors have read and agreed to the published version of the manuscript.

**Funding:** This research was funded by National Natural Science Foundation of China, grant number [61601468].

**Data Availability Statement:** Data is contained within the article.

**Acknowledgments:** This work was supported by the National Natural Science Foundation of China (No. 61601468); we thank Y. Liu (School of Microelectronics, Xidian University) for the use of CASTEP code in Materials Studio.

**Conflicts of Interest:** The authors declare no conflict of interest.

## References

1. Fan, Q.; Liu, H.; Jiang, L.; Zhang, W.; Song, Y.; Wei, Q.; Yu, X.; Yun, S. Three-dimensional metallic carbon allotropes with superhardness. *Nanotechnol. Rev.* **2021**, *10*, 1266–1276. [CrossRef]
2. Gao, Y.; Wu, Y.; Huang, Q.; Ma, M.; Pan, Y.; Xiong, M.; Li, Z.; Zhao, Z.; He, J.; Yu, D. First principles studies of superhard BC6N phases with unexpected 1D metallicity. *Comput. Mater. Sci.* **2018**, *148*, 157–164. [CrossRef]
3. Fan, Q.; Wu, N.; Yang, R.; Zhang, W.; Yu, X.; Yun, S. All $sp^2$ hybridization BN polymorphs with wide bandgap. *J. Appl. Phys.* **2022**, *131*, 055703. [CrossRef]
4. Liu, Y.; Li, X.; Xing, M.; Jin, J. Novel $BCN_2$ and CN compounds in *C*2/*m* phase: First-principle calculations. *J. Phys. Chem. Solids* **2021**, *158*, 110231. [CrossRef]
5. Li, X.; Xing, M. Two novel superhard monoclinic phase of B–C–N compounds. *J. Solid State Chem.* **2020**, *292*, 121750. [CrossRef]
6. Fan, Q.; Li, C.; Yang, R.; Yu, X.; Zhang, W.; Yun, S. Stability, mechanical, anisotropic and electronic properties of oP8 carbon: A superhard carbon allotrope in orthorhombic phase. *J. Solid State Chem.* **2021**, *294*, 121894. [CrossRef]
7. Qu, N.R.; Wang, H.C.; Li, Q.; Li, Y.D.; Li, Z.P.; Gou, H.Y.; Gao, F.M. Surperhard monoclinic $BC_6N$ allotropes: First-principles investigations. *Chin. Phys. B* **2019**, *28*, 096201. [CrossRef]
8. Li, S.; Shi, L. Two novel superhard structures: Monoclinic $BC_3N$. *Physica B* **2020**, *584*, 412061. [CrossRef]
9. Fan, Q.; Liu, H.; Jiang, L.; Yu, X.; Zhang, W.; Yun, S. Two orthorhombic superhard carbon allotropes: C16 and C24. *Diam. Relat. Mater.* **2021**, *116*, 108426. [CrossRef]
10. Zhu, H.; Shi, L.; Li, S.; Duan, Y.; Zhang, S.; Xia, W. Effects of hydrostatic pressure and biaxial strains on the elastic and electronic properties of *t*-$C_8B_2N_2$. *J. Appl. Phys.* **2018**, *123*, 135103. [CrossRef]
11. Wang, D.; Shi, R.; Gan, L.H. *t*-$C_8B_2N_2$: A potential superhard material. *Chem. Phys. Lett.* **2017**, *669*, 80–84. [CrossRef]
12. Fan, Q.; Liu, H.; Yang, R.; Yu, X.; Zhang, W.; Yun, S. An orthorhombic superhard carbon allotrope: *Pmma* $C_{24}$. *J. Solid State Chem.* **2021**, *300*, 122260. [CrossRef]
13. Wang, S.; Oganov, A.R.; Qian, G.; Zhu, Q.; Dong, H.; Dong, X.; Esfahani, M.M.D. Novel superhard B–C–O phases predicted from first principles. *Phys. Chem. Chem. Phys.* **2016**, *18*, 1859–1863. [CrossRef] [PubMed]
14. Fan, Q.; Wei, Q.; Chai, C.; Zhang, M.; Yan, H.; Zhang, Z.; Zhang, J.; Zhang, D. Elastic and electronic properties of *Imm*2- and *I*-4*m*2-BCN. *Comput. Mater. Sci.* **2015**, *97*, 6–13. [CrossRef]
15. Fan, Q.; Wei, Q.; Chai, C.; Yan, H.; Zhang, M.; Lin, Z.; Zhang, Z.; Zhang, J.; Zhang, D. Structural, mechanical, and electronic properties of *P*3*m*1-BCN. *J. Phys. Chem. Solids* **2015**, *79*, 89–96. [CrossRef]
16. Li, X.; Xing, M. Novel carbon-rich nitride $C_3N$: A superhard phase in monoclinic symmetry. *Comput. Mater. Sci.* **2019**, *158*, 170–177. [CrossRef]
17. Xing, M.; Li, X. $BC_2O$ in *C*2/*m* phase: Light element compound with direct band gaps. *J. Solid State Chem.* **2021**, *304*, 122590. [CrossRef]
18. Fan, Q.; Wei, Q.; Chai, C.; Yu, X.; Liu, Y.; Zhou, P.; Yan, H.; Zhang, D. First-principles Study of Structural, Elastic, Anisotropic, and Thermodynamic Properties of *R*3-$B_2C$. *Chin. J. Phys.* **2015**, *53*, 100601.
19. Fan, Q.; Zhao, Y.; Yu, X.; Song, Y.; Zhang, W.; Yun, S. Physical properties of a novel microporous carbon material. *Diam. Relat. Mater.* **2020**, *106*, 107831. [CrossRef]
20. Cui, H.J.; Yan, Q.B.; Sheng, X.L.; Wang, D.L.; Zheng, Q.R.; Su, G. The geometric and electronic transitions in body-centered-tetragonal C8: A first principle study. *Carbon* **2017**, *120*, 89–94. [CrossRef]
21. Xing, M.; Li, X. A porous nanotube network structure of metallic carbon. *Results Phys.* **2021**, *28*, 104579. [CrossRef]
22. Fan, Q.; Wei, Q.; Chai, C.; Yan, H.; Zhang, M.; Zhang, Z.; Zhang, J.; Zhang, D. Structural, anisotropic and thermodynamic properties of boron carbide: First principles calculations. *Indian J. Pure Ap. Phys.* **2016**, *54*, 227–235.
23. Yu, X.; Su, R.; He, B. A novel BN Polymorph with ductile manner. *J. Solid State Chem.* **2022**, *306*, 122794. [CrossRef]
24. Hohenberg, P.; Kohn, W. Inhomogeneous electron gas. *Phys. Rev.* **1964**, *136*, B864. [CrossRef]

25. Kohn, W.; Sham, L.J. Self-consistent equations including exchange and correlation effects. *Phys. Rev.* **1956**, *140*, A1133. [CrossRef]
26. Yu, X.; Su, R.; He, B.; Ma, B. Theoretical investigations of a BN polymorph with $sp^2$+$sp^3$ hybridizations. *Crystals* **2021**, *11*, 1574. [CrossRef]
27. Clark, S.J.; Segall, M.D.; Pickard, C.J.; Hasnip, P.J.; Probert, M.I.J.; Refson, K.; Payne, M.C. First principles methods using CASTEP. *Z. Kristallogr.* **2005**, *220*, 567–570. [CrossRef]
28. Perdew, J.P.; Burke, K.; Ernzerhof, M. Generalized gradient approximation made simple. *Phys. Rev. Lett.* **1996**, *77*, 3865. [CrossRef]
29. Ceperley, D.M.; Alder, B.J. Ground state of the electron gas by a stochastic method. *Phys. Rev. Lett.* **1980**, *45*, 566–569. [CrossRef]
30. Pfrommer, B.G.; Cote, M.; Louie, S.G.; Cohen, M.L. Relaxation of crystals with the quasi-Newton method. *J. Comput. Phys.* **1997**, *131*, 233–240. [CrossRef]
31. Vanderbilt, D. Soft self-consistent pseudopotentials in a generalized eigenvalue formalism. *Phys. Rev. B* **1990**, *41*, 7892–7895. [CrossRef] [PubMed]
32. Baroni, S.; de Gironcoli, S.; Corso, A.D.; Giannozzi, P. Phonons and related crystal properties from density-functional perturbation theory. *Rev. Mod. Phys.* **2001**, *73*, 515–562. [CrossRef]
33. Krukau, A.V.; Vydrov, O.A.; Izmaylov, A.F.; Scuseria, G.E. Influence of the exchange screening parameter on the performance of screened hybrid functionals. *J. Chem. Phys.* **2006**, *125*, 224106. [CrossRef] [PubMed]
34. Voigt, W. *Lehrburch der Kristallphysik*; Teubner, B.G., Ed.; Johnson Reprint Corp: Leipzig, Germany, 1928. (In German)
35. Reuss, A. Berechnung der Fließgrenze von Mischkristallen auf Grund der Plastizit€atsbedingung für Einkristalle. *Z. Angew. Math. Mech.* **1929**, *9*, 49–58. [CrossRef]
36. Hill, R. The elastic behaviour of a crystalline aggregate. *Proc. Phys. Soc. Lond.* **1952**, *65*, 349. [CrossRef]
37. Zhang, X.X.; Wang, Y.C.; Lv, J.; Zhu, C.Y.; Li, Q.; Zhang, M.; Li, Q.; Ma, Y.M. First-principles structural design of superhard materials. *J. Chem. Phys.* **2013**, *138*, 114101. [CrossRef] [PubMed]
38. Luo, X.; Li, L.; Wang, W.; Tian, Y. Superhard $B_2C_2N_2$ compounds from first-principles calculations. *J. Appl. Phys.* **2011**, *109*, 023516.
39. Wu, Z.J.; Zhao, E.J.; Xiang, H.P.; Hao, X.F.; Liu, X.J.; Meng, J. Crystal structures and elastic properties of superhard $IrN_2$ and $IrN_3$ from first principles. *Phys. Rev. B* **2007**, *76*, 054115. [CrossRef]
40. Fan, Q.Y.; Wu, N.; Chen, S.M.; Jiang, L.; Zhang, W.; Yu, X.H.; Yun, S.N. P213 BN: A novel large-cell boron nitride polymorph. *Commun. Theor. Phys.* **2021**, *73*, 125701. [CrossRef]
41. Qiao, L.; Hang, L.; Li, P.; Zhang, H.; Yan, G. Novel Carbon-Rich B−C Compounds in orthorhombic phase: First-principles calculations. *J. Solid State Chem.* **2021**, *300*, 122263. [CrossRef]
42. Dai, J.; Wu, X.; Yang, J.; Zeng, X.C. Porous Boron Nitride with Tunable Pore Size. *J. Phys. Chem. Lett.* **2014**, *5*, 393–398. [CrossRef] [PubMed]
43. Marmier, A.; Lethbridge, Z.A.D.; Walton, R.I.; Smith, C.W.; Parker, S.C.; Evans, K.E. ElAM: A computer program for the analysis and representation of anisotropic elastic properties. *Comput. Phys. Commun.* **2010**, *181*, 2102–2115. [CrossRef]
44. Fan, Q.Y.; Peng, H.C.; Zhang, W.; Yu, X.H.; Yun, S.N. Physical properties of group 14 elements in P2/m phase. *J. Solid State Chem.* **2022**, *305*, 122641. [CrossRef]
45. Ma, Z.Y.; Zuo, J.; Tang, C.Z.; Wang, P.; Shi, C.L. Physical properties of a novel phase of boron nitride and its potential applications. *Mater. Chem. Phys.* **2020**, *252*, 123245. [CrossRef]
46. Qiao, L.P.; Jin, Z.; Yan, G.Y.; Li, P.; Hang, L.M.; Li, L. Density-functional-studying of oP8–, tI16–, and tP4–$B_2CO$ physical properties under pressure. *J. Solid State Chem.* **2019**, *270*, 642–650. [CrossRef]
47. Fan, Q.; Zhao, R.; Zhang, W.; Song, Y.; Sun, M.; Schwingenschlögl, U. Low-energy $Ga_2O_3$ polymorphs with low electron effective masses. *Phys. Chem. Chem. Phys.* **2022**, *24*, 7045–7049. [CrossRef]
48. Xing, M.; Li, X. Designing $sp^3$ networks of two novel carbon allotropes in the *P*4/*mmm* phase. *Chin. J. Phys.* **2022**, *75*, 90–103. [CrossRef]
49. Fan, Q.; Hao, B.; Zhao, Y.; Song, Y.; Zhang, W.; Yun, S. Si–C alloys with direct band gaps for photoelectric application. *Vacuum* **2022**, *199*, 110952. [CrossRef]
50. Xing, M.; Qian, C.; Li, X. Two novel carbon allotropes with tetragonal symmetry: First-principles calculations. *J. Solid State Chem.* **2022**, *309*, 122971. [CrossRef]
51. Connétable, D.; Thomas, O. First-principles study of the structural, electronic, vibrational, and elastic properties of orthorhombic NiSi. *Phys. Rev. B* **2009**, *79*, 094101. [CrossRef]
52. Fan, Q.Y.; Wei, Q.; Yan, H.Y.; Zhang, M.G.; Zhang, Z.X.; Zhang, J.Q.; Zhang, D.Y. Elastic and electronic properties of *Pbca*-BN: First-principles calculations. *Comput. Mater. Sci.* **2014**, *85*, 80–87. [CrossRef]
53. Ravindran, P.; Fast, L.; Korzhavyi, P.A.; Johansson, B.; Wills, J.; Eriksson, O. Density functional theory for calculation of elastic properties of orthorhombic crystals: Application to $TiSi_2$. *J. Appl. Phys.* **1998**, *84*, 4891–4904. [CrossRef]